Journal of Colloid and Interface Science 677 (2025) 942–951

Contents lists available at ScienceDirect

Journal of Colloid And Interface Science

journal homepage: www.elsevier.com/locate/jcis

Regular Article

Dual-network hydrogel capsules for controlled molecular transport *via* pH and temperature responsiveness

Hui Yang [a,b], Catherine P. Whitby [b,c], Jadranka Travas-Sejdic [a,b,*]

[a] Centre for Innovative Materials for Health, School of Chemical Sciences, The University of Auckland, 23 Symonds Street, Auckland, New Zealand
[b] MacDiarmid Institute for Advanced Materials and Nanotechnology, Victoria University of Wellington, PO Box 600, Wellington, New Zealand
[c] School of Food Technology and Natural Sciences, Massey University, Palmerston North, New Zealand

GRAPHICAL ABSTRACT

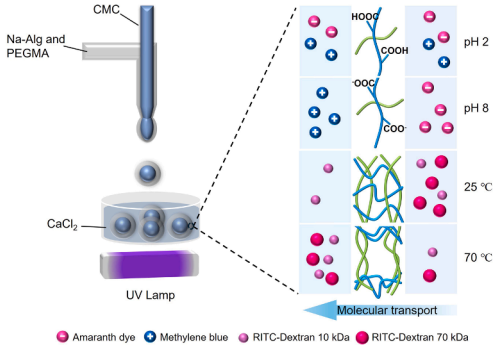

ABSTRACT

We have developed innovative core–shell hydrogel capsules with a dual-network shell structure designed for precise control of molecular transport in response to external stimuli such as pH and temperature. The capsules were fabricated using a combination of microfluidic electrospray techniques and water-in-water (w/w) core–shell droplets templating. The primary network of the shell, calcium alginate (Ca-Alg), with a pK_a around 3.4, exhibits sensitivity to pH. The secondary network of the shell, poly(ethylene glycol) methyl ether methacrylate (PEGMA), undergoes a volume phase transition near 60 °C. These properties enable precise molecular transport control in/out of the capsules by modulating the surface charges through varying pH and modifying pore size through temperature changes. Moreover, the dual-network shell structure not only significantly enhances the mechanical strength of the capsules but also improves their stability under external stimulus, ensuring structural integrity during the transport of molecules. This research lays the groundwork for further investigations into the multimodal stimuli-responsive hydrogel systems to control molecular transport, important in applications such as sensors and reactors for chemical cascade reactions.

1. Introduction

Hydrogels are three-dimensional structures created from hydrophilic polymers, interlinked through crosslinking, capable of absorbing and retaining substantial amounts of water while preserving their original framework [1,2]. A distinctive feature of hydrogels is their responsiveness to environmental stimuli [3,4], such as temperature [5], pH [6], light exposure [7], electric fields [8] or specific chemical interactions

* Corresponding author at: Centre for Innovative Materials for Health, School of Chemical Sciences, The University of Auckland, 23 Symonds Street, Auckland, New Zealand.
E-mail address: j.travas-sejdic@auckland.ac.nz (J. Travas-Sejdic).

https://doi.org/10.1016/j.jcis.2024.08.119
Received 16 July 2024; Received in revised form 12 August 2024; Accepted 15 August 2024
Available online 16 August 2024

[9], enabling them to adaptively alter their physical properties. However, stimuli-responsive hydrogels have certain limitations related to stability under environmental fluctuations [10], fabrication methodology [11] and molecular transport control [12]. For example, many hydrogels only respond to a single stimulus, which limits their functionality in environments where multiple stimuli are present, reducing their potential in the applications [13]. Additionally, Alginate hydrogels often lack the mechanical strength to withstand physical stresses, particularly in dynamic environments or applications involving mechanical manipulation [14,15]. Fabricating hydrogels that can respond to multiple stimuli in a controlled manner involves complex synthesis processes, requiring elaborate devices, delicate operation and careful consideration of hydrophilic properties [16]. One of the primary challenges of responsive hydrogels is achieving precise control over their responsiveness [17]. Many hydrogels do not differentiate well between different stimuli, leading to non-specific responses that can reduce the precision of molecular transport control [18]. To address these limitations, dual-network hydrogels have been developed to respond to multiple stimuli [19]. These hydrogels enhance precise control over molecular transport and improve stability [20], making them adapt to dynamic environments. Hydrogel capsules with a core–shell structure featuring a water core harness the intrinsic advantages of hydrogels, such as high water content [21] and protection of encapsulated substances [22], while bringing potential of multi-functional systems [23]. The capsule shell's network can be designed with pathways that respond to specific external stimuli, allowing for controlled transport of molecules [24].

Droplet microfluidics technology facilitates the controlled production of monodisperse droplets [25,26]. However, the process of forming a water-in-water (w/w) droplets is challenging due to the low interfacial tension between the aqueous phases, which can weaken the interactions at the interfaces, complicating the droplets formation process [27–29]. Advances in microfluidic electrospray technology present a promising way for w/w droplets [30] by introducing external electric forces to enhance droplet formation control, facilitating the production of droplets from two compatible aqueous solutions. This addresses the limitations in the choice of polymers and expands the potential utility of w/w droplets. Furthermore, hydrogel droplets can be rapidly gelled, which can stabilize the droplets and prevent any further mixing of the two solutions. Consequently, the microfluidic electrospray technique enables the production of capsules with well-defined hydrogel shells and water cores in a controlled manner [31–33].

Here, we utilized a microfluidic electrospray system to form capsules with a water core and dual-network hydrogel shell. The dual-network shell layer is composed of calcium alginate (Ca-Alg) and poly(ethylene glycol) methyl ether methacrylate (PEGMA), while the water core contains a carboxymethylcellulose sodium salt (CMC) solution. The pKa of CMC is generally around 4.3 to 4.5. For alginate, the pKa values are around 3.38 for mannuronic acid residues and 3.65 for guluronic acid residues. Given the similar pKa values of CMC and alginate, pH variations minimally affect the protonation and deprotonation of the hydrogel shell and core. This minimizes the impact of the CMC polymer in the core on dye partitioning between the core and shell phases. This dual network allows for the precise control of molecular transport based on the charge and molecular weight, in response to pH and temperature changes. Moreover, by adjusting the composition of the hydrogel, we enhance the transport efficiency and increase the mechanical strength and stability of the capsules. We believe that the dual-stimuli-responsive hydrogel capsules, which respond to two distinct stimuli, offer great potential for synergistic control over molecular transport. This makes them highly suitable to control processes in aqueous environments, such as in sensors that can detect changes in the environment [34] and designing capsule-based reactors for chemical cascade reactions [35–37].

2. Experimental section

2.1. Materials

Carboxymethylcellulose sodium salt (CMC) with a molecular weight of 90 kDa, PEGMA with a molecular weight of 300 Da, rhodamine isothiocyanate (RITC)-tagged dextran of molecular weights 10 kDa and 70 kDa, and N, N′-methylenebisacrylamide (MBAm) were procured from Sigma-Aldrich. Irgacure 2959, amaranth dye (AD) and methylene blue (MB) were obtained from AK Scientific. Sodium alginate (Na-Alg) with a molecular weight of 116–227 kDa was sourced from Duchefa Biochemie. Calcium chloride dihydrate ($CaCl_2{\cdot}2H_2O$) was acquired from Scharlau.

2.2. Fabrication of dual-network hydrogel capsules using a capillary microfluidic device

The microfluidic setup was constructed by fitting a tapered cylindrical capillary with a 300-μm orifice (outer diameter 1.0 mm, inner diameter 0.58 mm, sourced from Harvard Apparatus) inside a *T*-shaped plastic connector (inner diameter 1.2 mm, outer diameter 2.3 mm). This arrangement allowed the inner water phase to be fed through the capillary, while the outer water phase was introduced using a T connector. Flow rates for the inner and outer phases were set at 0.15 mL/min and 0.3 mL/min, respectively. A 5 kV high voltage (High voltage power supply series 230, sourced from Spellman's Bertan) between the needle of the shell phase (positive electrode) and a 1 % w/w $CaCl_2$ water bath (negative electrode) facilitated the formation w/w core–shell droplets. In this experiment, using sodium alginate solution droplets form when a positive electric potential is applied to the needle, Na^+ cations migrate quickly and are absorbed at the droplet surface [38]. The surface tension decreases leading to smaller droplets. The distance between the nozzle and $CaCl_2$ water bath is 5 cm. After alginate gelation, the core–shell capsules were photopolymerized using UV light. This process involves a 20-minute exposure to UV light, with an intensity of 680 mW/cm^2 and a wavelength of 365 nm (Zhongshan UV Lighting Company), to initiate the crosslinking of the PEGMA with MBAm within the hydrogel shell layer. Finally, the capsules were washed with distilled water several times and kept in water at room temperature.

2.3. Characterization

The size changes of hydrogel capsules under varying pH levels and temperatures were monitored and captured using an optical microscope (Leica M205 FA). A Malvern Zetasizer was used to obtain the zeta potential of the dual-network hydrogel with varying concentrations of MBAm (0, 0.5, 1.5, and 2.5 % w/w) in an aqueous solution with pH 2 and pH 8. The UV/Vis spectrophotometer (Shimadzu UV-3600) with a temperature control unit (Shimadzu TCC-100) measured the Lower Critical Solution Temperature (LCST). The charge-selective transport properties of the capsules, at varying pH levels, were investigated using the UV–Vis spectrophotometer (NanoPhotometer® NP80) by measuring the absorbance changes of AD and MB at their respective peak wavelengths. Temperature-dependent size-selective properties were investigated using a spectrofluorometer (Jasco FP-8600) by recording the fluorescence intensity variations of RITC-Dextran dyes. A universal testing machine (INSTRON 5943) was used to evaluate the mechanical properties of the hydrogel networks with varying degrees of crosslinking.

3. Results and discussion

3.1. Fabrication of dual-network hydrogel capsules

Water-in-water hydrogel droplets, dispersed within a continuous aqueous phase, represent a unique class of w/w/w systems. The ability to engineer and control multiple aqueous phase droplets opens new

possibilities in various fields. Here, we employed a capillary microfluidic electrospray device to fabricate multiple w/w phase 'capsules' with a dual-networks hydrogel shell, that respond to pH and temperature variations, and an aqueous core (Fig. 1a). Thus, this method produces uniform core–shell capsules with an aqueous environment both inside and outside the capsules, without involving an oil phase and any additional steps to remove the oil shell. The w/w/w core–shell droplets are initially formed using two syringe pumps, followed by gelation with a $CaCl_2$ solution. The pumps deliver the core fluid, consisting of a 1 % w/v CMC aqueous solution, and the shell fluids, which are composed of 1.5 % w/v Na-Alg, 10 % w/v PEGMA, 0.5 % w/v Irgacure 2959, and varying concentrations of MBAm of 0 %, 0.5 %, 1.5 %, and 2.5 % w/v aqueous solutions, through the concentric channels of a coaxial needle. An electric field, applied between the needle of the shell phase and $CaCl_2$ water bath by a voltage generator, causes the concentric drops of the two fluids at the tip of the needle to break up into droplets due to the balance of forces, including surface tension and electrostatic repulsion [39]. Both Na-Alg and CMC are polysaccharides that form highly viscous solutions in water. In the microfluidic system, this high viscosity prevents immediate mixing when the solutions meet, allowing for the formation of distinct phases and time for the crosslinking of the polymers in the shell. In the process, the w/w droplets were electrosprayed into a gelation bath of a 1 % w/w aqueous solution of $CaCl_2{\cdot}2H_2O$. Alginate, a polysaccharide derived from brown seaweed, consists of mannuronic and guluronic acid blocks. The Ca^{2+} ions act as bridges between the alginate chains, specifically binding to the guluronic acid blocks in alginate [40], which leads to the formation of a three-dimensional Ca-Alg gel network. PEGMA is a methacrylate (MA) monomer with a poly (ethylene glycol) (PEG) pendant chain where the PEG chains provide flexibility and hydrophilicity, while the MA group allows for polymerization and copolymerization in the presence of MBAm [41]. The polymerization process is initiated by a photoinitiator, Irgacure 2959, and exposure to UV light, which leads to the formation of a crosslinked p (PEGMA-*co*-MBAm) network (noted as 'p(PEGMA)' for simplicity). Therefore, the secondary p(PEGMA) network forms within the already established primary Ca-Alg network, resulting in a dual-network structure. The size distribution of the formed Alg, D-0.5 %, D-1.5 %, and D-2.5 % hydrogel capsules is shown in Fig. S1. All the capsules show size coefficient of variation (CV) for the size of the capsules below 5 %, indicating that the capsules are highly monodisperse. The diameter of the core relative to the entire system is approximately 84 %, while the core's relative volume is about 60 % of the total system volume (Fig. S2). The applied voltage is crucial in the electrospraying process, as it determines the formation of the Taylor cone at the nozzle tip essential for generating fine droplets. The size of the hydrogel capsules ranged from 4.1 mm at 0 kV potential to 1.5 mm at 10 kV (Fig. S3a). Increasing the potential further resulted in the formation of unstable liquid jets, which disintegrated into multiple microscopic droplets. The distance between the nozzle and $CaCl_2$ water bath also plays a significant role. The electric field strength E in an electrospray system is given by the formula $E=V/d$, where V is the applied voltage and d is the distance between the nozzle and the $CaCl_2$ solution. The data on the droplets' size range *v.s.* nozzle-solution distance is presented in Fig. S3b. When the distance is maintained at 5 cm, the droplet size is approximately 3.08 mm. Decreasing the distance to 3 cm reduces the droplet size to 2.48 mm, while increasing the distance to 7 cm enlarges the droplet size to 3.23 mm. Additionally, the setup can be easily adjusted to use, for example, a nozzle of a smaller diameter of 0.45 mm and higher voltages 5 kV could be applied to decrease the size to microliter range (Fig. S4). In our electrospray system, both the shell (alginate) and core (CMC) phases exhibit lower interfacial tension compared to oil–water systems. This lower interfacial tension in the w/w system leads to less stable droplets that are more prone to deformation. Unlike oil–water droplets, which form nearly perfect spheres due to higher surface tension (see Fig. S5a for the water–oil droplets composed of a paraffin oil core and alginate shell, as an example to demonstrate the point), alginate and CMC droplets tend to form less regular shapes (Fig. S5b). The CMC core, however, maintains its phase well due to its high viscosity.

3.2. Comparative analysis of single and dual-network hydrogels

Firstly, the dual-network hydrogel particles, consisting of Ca-Alg and p(PEGMA) (without the CMC water core) were investigated. These were categorized based on the concentration of the MBAm crosslinker: 0.5 %, 1.5 % and 2.5 % w/w MBAm (termed D-0.5 %, D-1.5 % and D-2.5 %, respectively). The 'control' sample was pure Ca-Alg hydrogel particles.

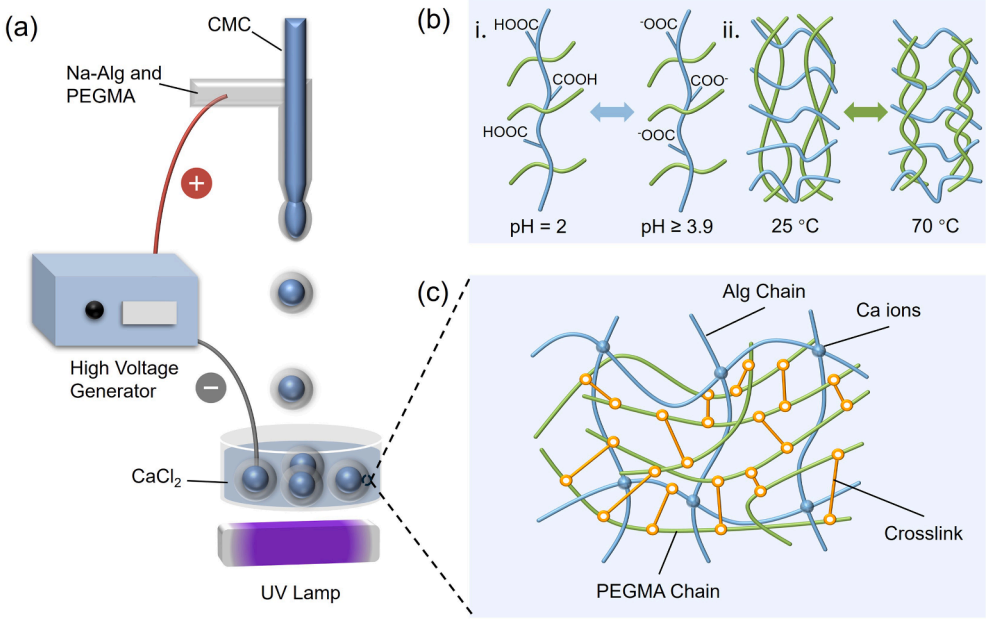

Fig. 1. Overview of hydrogel capsule fabrication and their response to pH and temperature variations. (a) Schematic of the electrospray microfluidic device illustrating the formation of dual-networks hydrogel capsule. (b) i. Schematic showing the protonation of the Ca-Alg network at pH 2 and deprotonation at pH ≥ 3.9. ii. Schematic depicting the capsules' response to temperature changes from 25 ℃ to 70 ℃ due to PEGMA temperature response. (c) Schematic of the dual hydrogel network shell, consisting of Ca-Alg and p(PEGMA), detailing the crosslinked networks.

We selected 50 particles from each group and dispersed them in pH 2 and pH 8 aqueous solution for up to 8 h. The single network Ca-Alg capsules exhibited approximately 25 % shrinkage at pH 2 compared to pH 8, while dual network capsules showed less than 7 % shrinkage (Fig. 2a). This behavior can be attributed to the protonation and deprotonation of the Ca-Alg hydrogel network [42]. At pH 2, the carboxylic acid groups within the Ca-Alg network undergo protonation, reducing electrostatic repulsion and enhancing hydrogen bonding. Conversely, at higher pH levels, the deprotonation of carboxyl groups increases the negative charge, promoting electrostatic repulsion among the polymer chains. The diameter change in dual-network particles is significantly less than in single-network particles, indicating that dual networks are more stable under varying pH environments while maintaining pH responsiveness. To evaluate the temperature-responsive behavior of hydrogel particles, we incubated particles with varying amounts of MBAm in water at different temperatures. Using bright-field microscopy, we tracked the size changes of these particles as the temperature increased from 25 °C to 70 °C. All particles show a slight decrease in diameter when heated (Fig. S6). Additionally, we use image J to track the grey value changes of the particles' images at 25 °C and 70 °C to compare their temperature-responsiveness. At 25 °C, the hydrogel network is more expanded, allowing more light to pass through, which makes the particles appear lighter. When the temperature is increased to 70 °C, the p(PEGMA) network shrinks and densifies, resulting in a darker appearance. This change in grey value effectively demonstrates the temperature-dependent behavior of the hydrogel particles (Fig. S7). At 25 °C, the grey value decreased from 127 to 90 when comparing hydrogel particles with a single alginate network to those with a dual network with 2.5 % w/w MBAm, likely due to the denser structure formed with increasing MBAm. When the temperature increased to 70 °C, the grey value of single alginate networks decreased by 13 %, indicating some degree of shrinkage. The dual network hydrogel with 0.5 % MBAm exhibited the most significant change due to the highest extent of phase transition [43], with a 63 % decrease in grey value, while those with 1.5 % w/w and 2.5 % w/w MBAm showed decreases of 35 % and 20 %, respectively. This behavior is attributed to the denser networks of the shells with higher MBAm concentration, which restrict the movement and conformational changes of the PEGMA chains, limiting the temperature-responsive property.

The mechanical properties of hydrogel particles were evaluated using a compression strain–stress test on individual capsules in an air setting [44]. Hydrogel particles, each 4 (±0.15) mm in diameter, were placed on a PMMA plate and compressed up to 30 % of their original height by another PMMA plate while the required compression force was measured. Fig. 2c shows that the mechanical properties of the particles are enhanced with increasing MBAm concentration in hydrogel particles. By analyzing the linear portion of the compression stress–-strain curve (specifically the strain from 0 to 15 %), Young's modulus was determined from the slope. The resulting values are 26.9, 30.3, 32.6 and 37.1 kPa for hydrogel particles with MBAm contents of 0, 0.5, 1.5, and 2.5 % w/w, respectively [45]. The increase in modulus is attributed to the formation of a denser crosslinked network within the hydrogel at higher MBAm concentrations, which restricts polymer chain mobility, making the hydrogel less flexible and more resistant to external forces [46]. The water content of hydrogel particles was evaluated by weighing the particles before and after freeze-drying. The water content decreased from 98 % to 90 % as the MBAm concentration increased from 0 to 2.5 % w/w (Fig. 2d) due to a more densely crosslinked hydrogel network slightly reducing the capacity to retain water. Nonetheless, all hydrogels maintained a high water content, highlighting their inherent

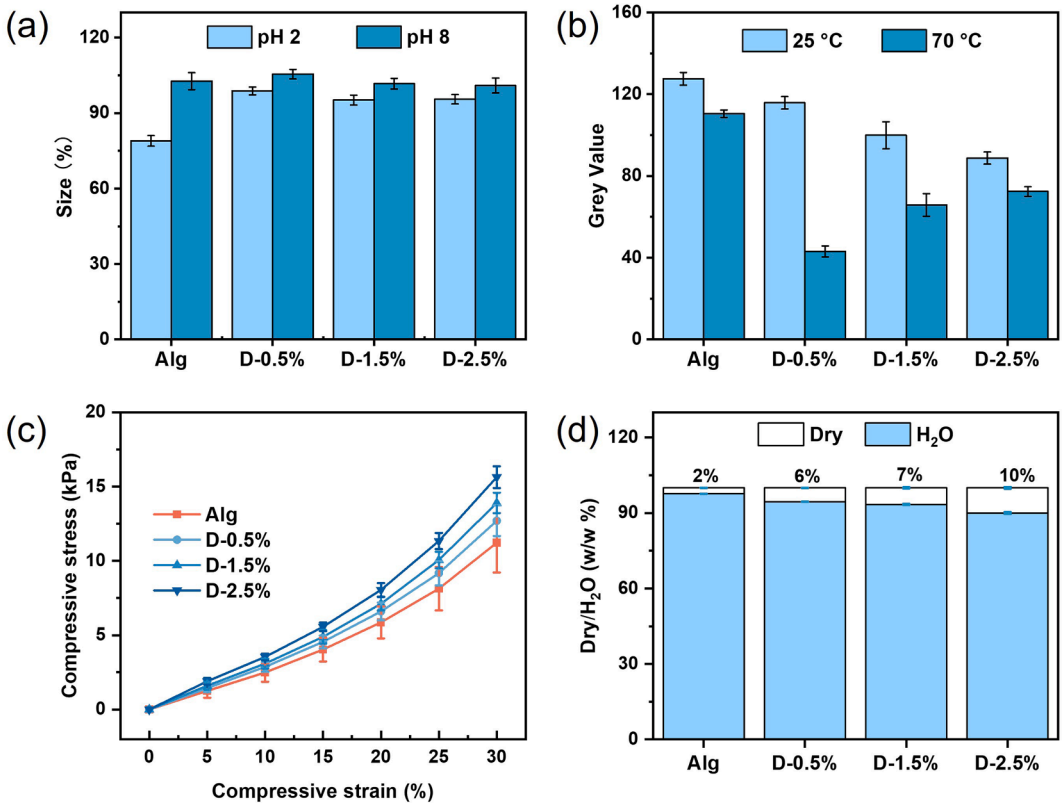

Fig. 2. (a) Size variation of hydrogel particles with varied MBAm content (0, 0.5, 1.5, and 2.5 % w/w) at pH 2 and 8. (b) Grey values of hydrogel particles with varied MBAm content (0, 0.5, 1.5, and 2.5 % w/w) in response to temperature of 25 ℃ and 70 ℃. (c) Mechanical behavior of hydrogel particles with varied MBAm content (0, 0.5, 1.5, and 2.5 % w/w) under compression at a constant compression speed of 10 μm/s. (d) Mass composition of hydrogel particles with varied MBAm content (0, 0.5, 1.5, and 2.5 % w/w), including dry weight and water. "Alg" refers to hydrogel particles formed solely from Ca-Alg networks, "D" represents dual-network hydrogel composed of Ca-Alg and p(PEGMA) with varying amounts of MBAm crosslinkers.

hydrophilicity [47].

The above suggests that the dual-network hydrogel particles exhibit dual responsiveness to both pH and temperature changes and enhanced mechanical strength while maintaining a high-water content.

3.3. The effect of crosslinking density on the molecular transport in the core–shell capsules

We next investigated the transport kinetics of methylene blue (MB) and amaranth dye (AD) into the hydrogel core–shell capsules, focusing on the effect of varying MBAm concentrations. MB (with a cationic $–NH_2$ group) and AD (with an anionic $–SO_3H$ group) were selected to study the pH effect because their charges interact significantly with the carboxyl (–COOH) groups on the alginate hydrogel which can be protonated or deprotonated depending on the pH. This interaction is crucial for understanding the electrostatic effects on the kinetics of dye uptake within the hydrogel particles. Initially, 50 capsules from each group were immersed in pH 8 and pH 2 solution to ensure full deprotonation or protonation of the carboxylic acid groups on Ca-Alg networks. Subsequently, the capsules were transferred to 5 mL of fresh pH 8 or pH 2 solutions, and 0.2 mg of AD and 0.04 mg MB were introduced to each group. Using the calibration curve for MB in aqueous pH 8 solution and AD in aqueous pH 2 solution (Fig. S8), we quantified the depletion in dye concentrations in the solutions and the corresponding increase in dye concentration within the hydrogel capsules. Fig. 3a and b present the changes in MB and AD concentrations over time in both the solution and inside the capsules with different MBAm concentrations in their shells (0, 0.5, 1.5 and 2.5 % w/w). For MB transport in the pH 8 solution, both single and dual networks hydrogel capsules exhibit a similar transport pattern. Most MB was transported into the capsules within the first hour, with the exterior solution concentrations decreasing from 8.2 ppm to less than 2 ppm, while the interior capsules' concentration increased to more than 70 ppm. For AD transport in the pH 2 solution, 'Alg' and 'D-0.5 %' capsules showed rapid dye uptake within the first half hour, saturating at around 40 ppm and 55 ppm, respectively. During the same period, the external solution concentrations of AD reduced from 39 ppm to 37 ppm and 36 ppm, respectively. In contrast, the 'D-1.5 %' and 'D-2.5 %' hydrogel capsules exhibited a gradual increase in dye concentration over the first 4 h, peaking at around 225 ppm and 200 ppm after 8 h, respectively, while the external solution concentrations dropped from 39 ppm to 21 ppm and 24 ppm, respectively.

The adsorption kinetic curves are shown in the Table S1, Fig. S9 and Table S2, Fig. S10. The kinetic curves were fitted with the pseudo-first-order [48], pseudo-second-order [49], intraparticle diffusion [50] and Elovich models [51]. For the AD and MB transport process, the correlation coefficient (R^2) values for the pseudo-second-order kinetic model were very close to 1. Furthermore, the value of $q_{e\ cal}$, calculated from the pseudo-second-order kinetic model, showed good agreement with the experimentally measured q_e, exp values. These results indicate that the pseudo-second-order model provided the best fit for the AD and MB transport into the capsules under pH variations. This suggests that AD and MB transport into the hydrogel capsules involves more than a simple

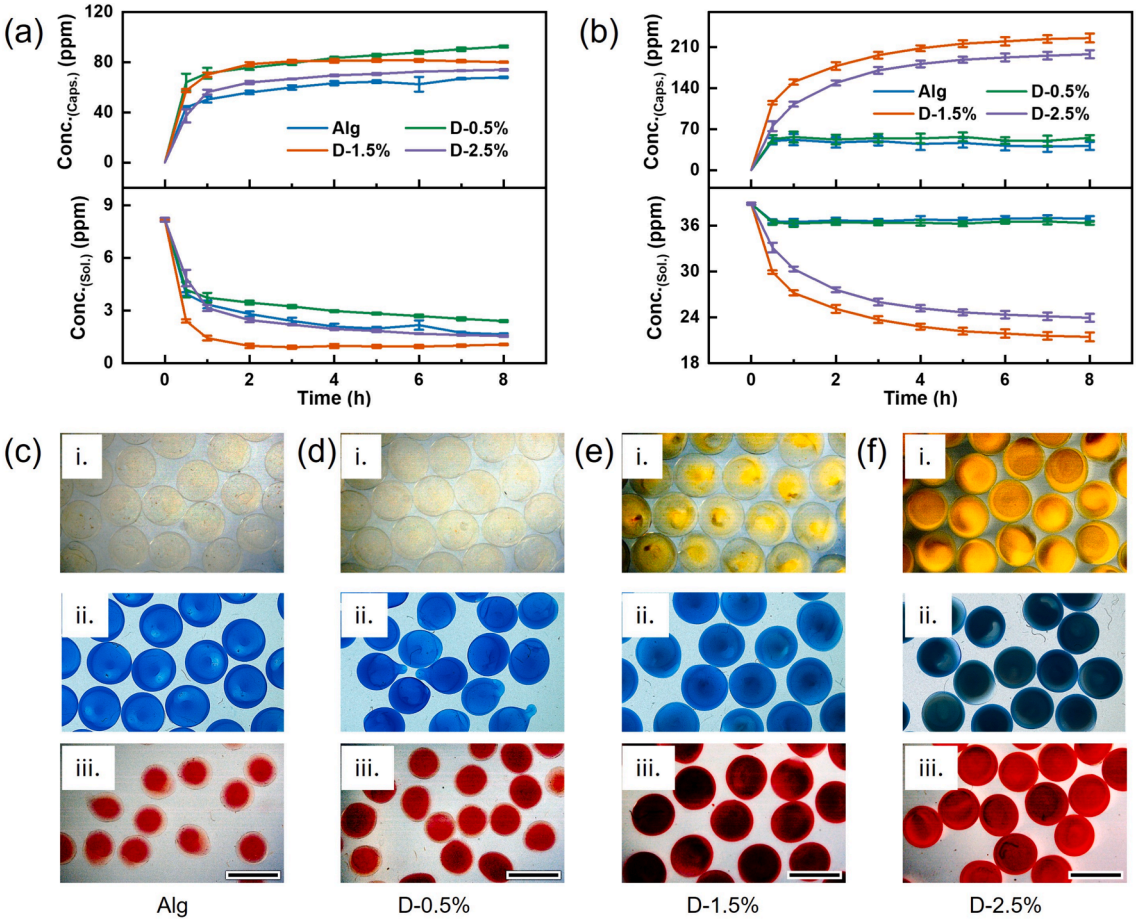

Fig. 3. (a) Kinetics of MB concentration changes in the solution and within the capsules containing varying amounts of MBAm at pH 8. (b) Kinetics of AD concentration changes in the solution and within the capsules containing varying amounts of MBAm at pH 2. (c) Microscopy images of capsules with a single Ca-Alg network: (i) as prepared in DI H_2O, (ii) after absorbing MB at pH 8, and (iii) after absorbing AD at pH 2. (d–f) Microscopy images of hydrogel capsules with varying MBAm concentrations (0.5, 1.5, and 2.5 % w/w): (i) as prepared in DI H_2O, (ii) after absorbing MB at pH 8, and (iii) after absorbing AD at pH 2. The scale bar is 3 mm.

physical adsorption process. The adsorption of ionic dyes onto the hydrogel surface is primarily influenced by the surface charge on the hydrogel, which depends on the solution's pH [52]. For hydrogel particles containing varying amounts of MBAm, zeta potential measurements show a stronger negative charge of around −30 mV at pH 8 and a near-neutral charge of around −5 mV at pH 2 (Fig. S11). In the context of MB transport into the hydrogel capsules, the transport is facilitated by the formation of an ionic complex between the imine groups of MB and the ionized carboxylic groups of alginates [53]. At pH 8, the electrostatic attraction force between the MB molecule and the alginate hydrogel surface is enhanced [54], resulting in increased MB absorption into the hydrogel capsules. In contrast, in the context of AD transport at pH 2, the surface charge density on the hydrogel decreases, resulting in a nearly neutral surface charge [55]. This neutralization reduces electrostatic repulsion, allowing negatively charged AD to pass through the dual-network shell of the capsules. Initially, the concentration gradient serves as the primary driving force for the AD molecules to transport into hydrogel capsules [56].

For the Alg and D-0.5 % capsules, the dye concentrations in both the exterior and interior were similar, indicating that a dynamic equilibrium had been achieved. However, for the D-1.5 % and D-2.5 % capsules, the dye concentration inside the capsules was significantly higher than outside after 8 h. This phenomenon can be explained by considering the complexities of dual-network crosslinking. The Elovich model, which further describes the pseudo-second-order kinetic on energetically heterogeneous sorbent surfaces [57], provided a good fit to D-1.5 % M and D-2.5 % hydrogel capsules. Varying the crosslinking density influences both the diffusivity and accumulation of molecules within hydrogels [58]. Increasing MBAm concentration leads to a denser network which may provide more binding sites for dye molecules, thereby enhancing their concentration within the capsules. Additionally, a higher crosslinking density is likely to introduce more energetic diversity across the dual hydrogel surface [59–61], generating varied types of binding sites favorable for dye adsorption [62]. Moreover, the presence of a water core in the hydrogel capsules increases the water content (Fig. S12a), allowing greater uptake of water-soluble dye, as the water core can accommodate more dye molecules compared to hydrogel particles with a crosslinked network core [63]. Furthermore, the water core containing AD is noticeably more colorful than the hydrogel alginate shell (Fig. S12b, ii), indicating higher dye accumulation in the core.

3.4. Controlling transport of different charged molecules under pH stimuli

The transport efficiency of AD and MB into the hydrogel capsules was investigated under various pH stimuli. 50 dual-network hydrogel capsules, each containing 1.5 % w/w MBAm, were placed into fresh 5 mL solutions containing 0.2 mg AD or 0.04mg MB at their respective pH 2 and 8. We monitored the changes in absorbance of the supernatant over 8 h to determine the decrease in the dye concentrations in the supernatant and the corresponding increase in the dye concentrations within the hydrogel capsules.

Based on the adsorption kinetic studies shown in Table S3 and Figs. S13 and S14, the pseudo-second-order model provided the best fit for the AD and MB transport under pH variations. For the transport

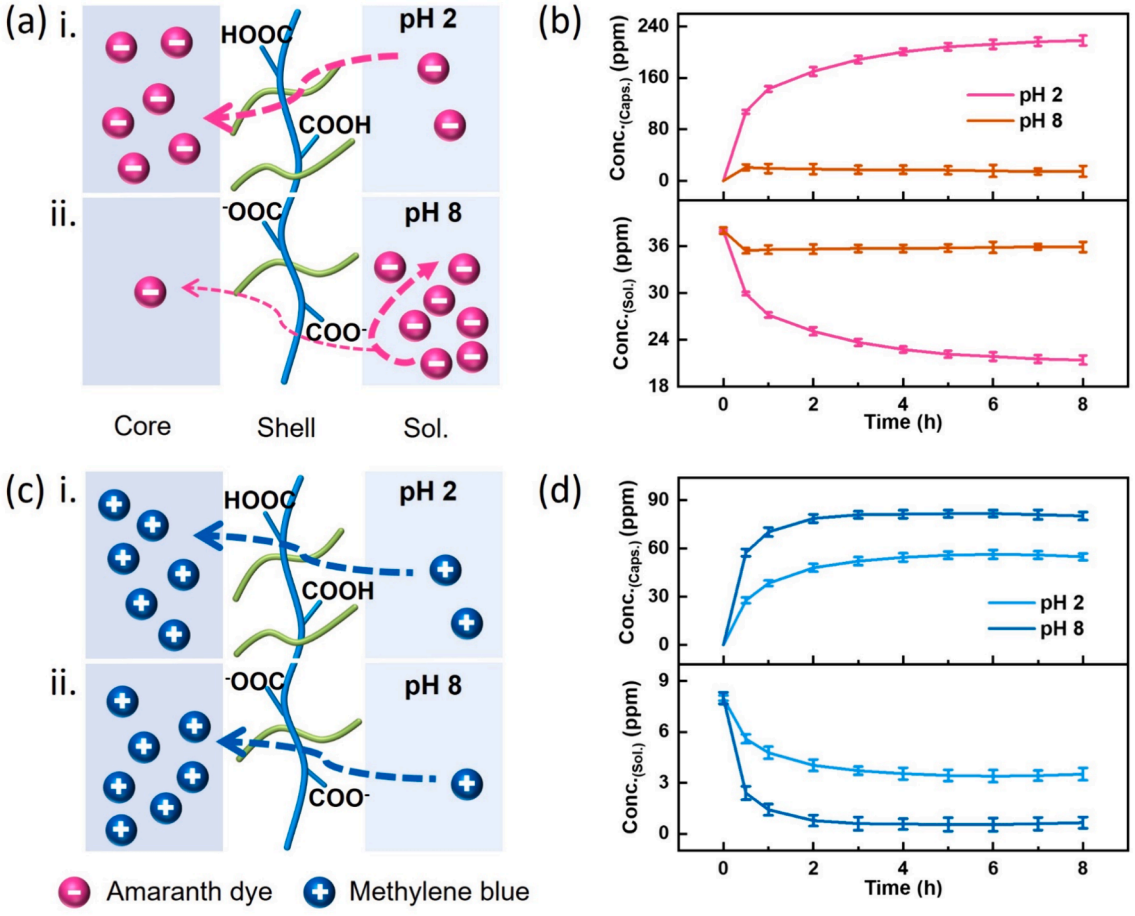

Fig. 4. (a) and (c) Schematic of the selective transport of AD (a) and MB (c) into hydrogel capsules at pH 2 (i) and pH 8 (ii). (b) and (d) The kinetics of permeation for AD (b) and MB (d) into capsules under the two pH conditions, presented as the concentrations of the dyes in the solution ($conc._{sol}$) and within the capsules ($conc._{caps}$) over 8 h. The anionic dye AD is represented by a purple sphere and the cationic dye MB is represented by a blue sphere. (For interpretation of the references to colour in this Fig. legend, the reader is referred to the web version of this article.)

efficiency of AD at pH 8, the internal concentration increases slightly from 0 ppm to just over 15 ppm, while the supernatant concentration decreases from approximately 38 ppm to 36 ppm (Fig. 4b). At this pH, the deprotonation of the COOH groups on the hydrogel's Ca-Alg network results in a highly negatively charged surface (around −30 mV). The increasing electrostatic repulsion between the negatively charged AD molecules and the hydrogel capsules leads to minimal AD uptake. Despite the concentration gradient promoting dye transport into the capsules, electrostatic repulsion remains the predominant factor influencing AD transport into the hydrogel capsules. At pH 2, the protonation of the COOH groups within the hydrogel's Ca-Alg network reduces electrostatic repulsion, thus allowing AD uptake. Additionally, the denser network of the capsules' shell with a high concentration of MBAm may be providing more binding sites for dye uptake, as discussed above. As a result, the concentration of AD within the capsules rises sharply from 0 ppm to over 200 ppm, while the concentration in supernatant decreases from approximately 38 ppm to 21 ppm (Fig. 4b). For the transport efficiency of MB, strong electrostatic interactions occurred between the positively charged MB dyes and the negatively charged dual hydrogel capsules at pH 8. This is demonstrated by the increased transport efficiency, with the concentration of MB inside the capsules rising from 0 ppm to about 80 ppm, and the concentration in supernatant decrease from around 8 ppm to 1 ppm (Fig. 4d), indicating the near-complete absorption of MB by the hydrogel capsules. In contrast, at pH 2, the protonation of the COOH groups allows H^+ ions to compete effectively with dye cations, decreasing the amount of dye adsorbed[52]. Consequently, the concentration inside the capsules increases from 0 ppm to over 55 ppm, while the concentration in supernatant decreases from approximately 8 ppm to 4 ppm (Fig. 4d). A further discussion on AD and MB concentrations in the core and shell of the hydrogel capsules is provided in Figs. S15 and S16. Therefore, pH effectively controls the selective transport of negatively charged AD and regulates the amounts of positively charged MB through the dual-network hydrogel capsules.

3.5. Controlling transport of dextran molecules of different molecular weights under temperature stimuli

The transport efficiency of RITC-Dextran with varying molecular weights 10 kDa and 70 kDa into D-1.5 %M was investigated under different temperature stimuli with pH 6.92. RITC-Dextran was chosen to study the effect of temperature because of the zwitterionic nature of RITC-Dextran, which minimizes the influence of electrostatic interactions with the hydrogel. This allows for a clearer observation of how temperature alone affects the kinetics of uptake, without the interferences due to charge interactions. Additionally, since the sizes of RITC-Dextran are around 2.77 nm for 10 kDa and 5.29 nm for 70 kDa, their uptake into the capsules provided an insight into the size threshold for molecular uptake by the hydrogel capsules at different temperatures.

Initially, hydrogel capsules were dispersed in deionized water at 25 ℃, where their diameters and weights were measured. The capsules were then heated to 70 °C, followed by measurement of their diameter and weight. Upon raising the temperature from 25 °C to 70 °C, a 20 % reduction in water content was observed. This significant water loss in the dual-network hydrogel was attributed to the hydrophobic behavior of the p(PEGMA) network, which shows phaser transitions at higher temperatures [41]. Further investigation of the LCST was carried out on hydrogels with similar compositions to the hydrogel capsules (Fig. 5b). Unlike in the capsules, the alginate in the Na-Alg/p(PEGMA) hydrogel was not crosslinked. Using UV–Vis spectroscopy, the LCSTs were determined to be approximately 59 °C for Na-Alg/p(PEGMA) and 70 °C for Ca-Alg/p(PEGMA). This difference is likely due to the added mechanical stiffness and the constraints imposed by the cross-linked structure of the Ca-alginate, which restricts the movement and conformational changes of the PEGMA chains [64,65]. It is important to note that the diameters of the capsules did not reflect this change (Fig. 5a), likely due to the low precision of measuring the diameter of the capsules (±80 μm). Combining the information above, the observed reduction in water content could be due to the contraction of the alginate and p(PEGMA) networks at higher temperatures. This might lead to an increase in pore size and capacity within the hydrogel structure, thereby increasing the transport efficiency at higher temperatures.

Next, 50 D-1.5 % capsules were dispersed in RITC-Dextran solutions of either 10 kDa and 70 kDa RITC-Dextran, at various temperatures and pH 6.92. The changes in the fluorescence intensity of the supernatant were monitored over 8 h. The calibration curves for both dyes (Fig. S17) were used to determine the decrease in the dye concentrations in the supernatant and the corresponding increase within the hydrogel capsules (Fig. 6b and d). For the 10 kDa RITC-Dextran, equilibrium was reached within 3 h. The dye concentration outside the capsules decreased from approximately 100 ppm to 90 ppm, while increased inside the capsules from 0 ppm to about 90 ppm. In contrast, the 70 kDa RITC-Dextran required 5 h to reach equilibrium, with the external concentration decreasing from about 78 ppm to 75 ppm, and the internal capsules' concentration increasing from 0 ppm to around 26 ppm. When examining the transport of molecules at 70 °C, we observed that most of the RITC-Dextran molecules rapidly transported into D-1.5 % capsules within the first half hour and then gradually approached equilibrium. For the 10 kDa RITC-Dextran, the exterior solution concentration decreased from about 88 ppm to 63 ppm, with the interior capsules' concentration rising from 0 ppm to 260 ppm. For the 70 kDa RITC-Dextran, the exterior solution concentration decreased from around 107 ppm to 85 ppm, and the interior concentration increased from 0 ppm to approximately 230 ppm. In conclusion, at the low temperature, the transport of dextran molecules into the D-1.5 % is more gradual and less efficient. However, at elevated temperatures, permeability

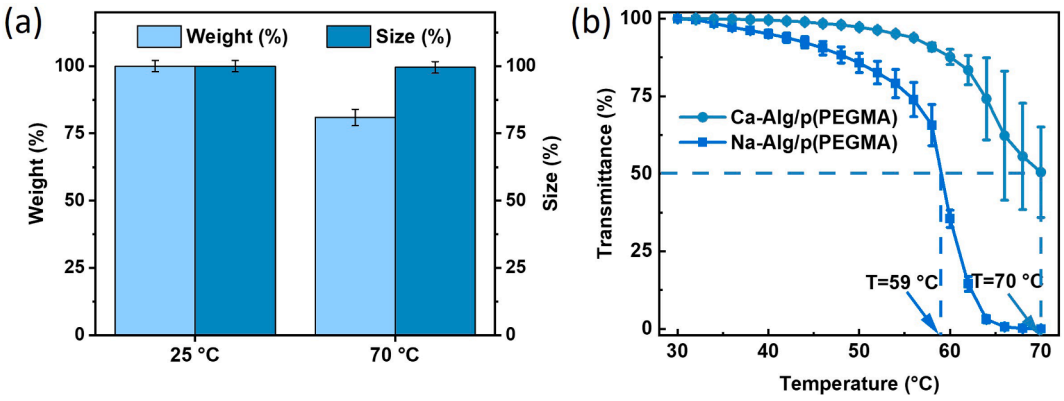

Fig. 5. (a) Changes in water content and size of D-1.5 % when subjected to temperature increase from 25 °C to 70 °C. (b) LCSTs of Na-Alg/p(PEGMA) and Ca-Alg/p(PEGMA) hydrogels, determined by UV–Vis spectroscopy at 500 nm.

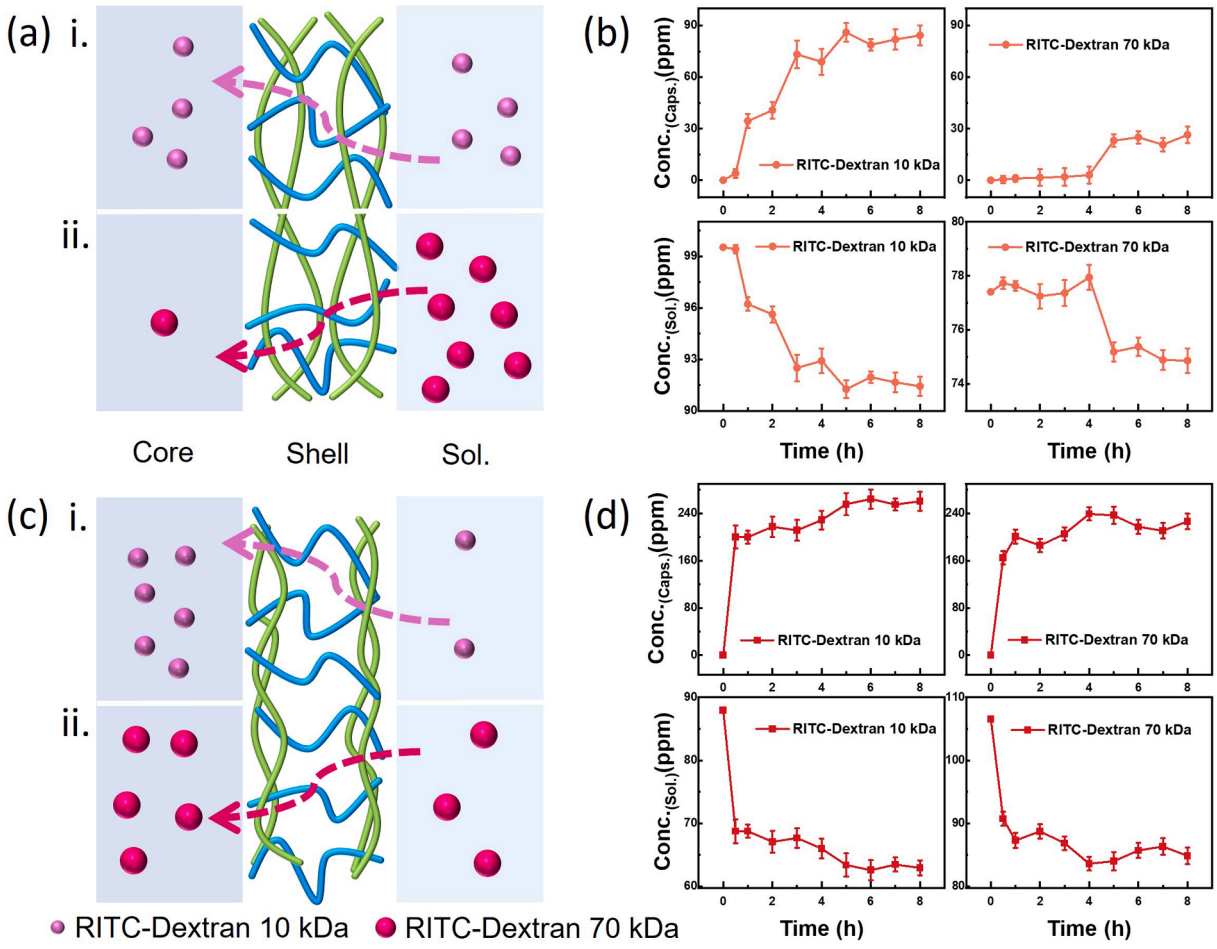

Fig. 6. Effect of temperature of 25 ℃ and 70 ℃ on the transport of 10 kDa and 70 kDa RITC-Dextran through hydrogel capsules. Schematics depicting the permeation processes for 10 kDa and 70 kDa RITC-Dextran in D-1.5 % capsules at 25 ℃ (a) and 70 ℃ (c). The kinetics of permeation for 10 kDa and 70 kDa RITC-Dextran in D-1.5 % capsules at 25 ℃ (b) and 70 ℃ (d).

significantly increases, enabling a quicker and greater uptake of both 10 kDa and 70 kDa dextran molecules, thus highlighting the temperature-selective transport properties of the D-1.5 % capsules. As the diffusion coefficient is proportional to the absolute temperature, the difference between 298 K and 343 K can only explain a 15 % difference in kinetics (according to Stokes-Einstein equation). Since the observed difference in kinetics is significantly greater, other factors besides temperature are contributing to this difference, the main one being the phase transition (collapse) of the PEGMA hydrogel at 70 ℃ which greatly affects the pore size of the capsules' shell.

The adsorption kinetic studies, shown in Table S4 and Fig. S18 indicate that none of the models investigated above fit the data of 10 and 70 kDa RITC-Dextran transport process at 25 °C. However, the transport process fits the pseudo-second-order kinetic model at 70 °C. At 25 °C, the smaller pore size of the hydrogel restricts the movement of the dye molecules, leading to slower diffusion and less interaction between zwitterionic RITC-Dextran and the hydrogel network. This restriction may cause a deviation from any specific kinetic model because the transport mechanism involves a mix of limited diffusion and weak adsorption interactions. Initially, the transport of RITC-Dextran molecules due to the concentration gradient from the outside solution to the inside, continuing until the gradient is minimized. For the 10 kDa RITC-Dextran, equilibrium is achieved when the concentrations inside and outside are similar. In contrast, for the 70 kDa RITC-Dextran, equilibrium is achieved while concentration gradient still exists, with the exterior concentration remaining significantly higher than interior. This suggests that the pore threshold in D-1.5 % is close to 70 kDa. When temperature increased to 70 °C, a significantly higher amount of dye was transported into the hydrogel capsules compared to the results obtained at 25 °C. This can be attributed to the temperature responsiveness of p (PEGMA) [66]. The alginate and PEGMA networks within the capsule shells undergo shrinking at 70 °C, leading to the formation of larger pores and increased capacity within the dual-network hydrogel due to the minimal changes in diameter. This restructuring increases the threshold of the capsules for RITC-Dextran molecules to pass through the capsule shell. Furthermore, increasing the temperature decreases the viscosity of CMC core solution, which may reduce the resistance for Dextran transport into the core of the capsules, leading to an increased uptake of Dextran dyes at 70 °C [67]. A further discussion on RITC-Dextran concentrations in the core and shell of the hydrogel capsules is provided in Fig. S19. In summary, temperature effectively controls the transport efficiency of molecules with different molecular weights into the dual-network hydrogel capsules.

4. Conclusion

This study introduces hydrogel capsules with a dual-network shell and a water core, fabricated using a combination of microfluidic electrospray technique and w/w/w core–shell droplets, and engineered with dual responsiveness to pH and temperature. The dual-network shell responsiveness originates from the pH sensitivity of the Ca-Alg network and the temperature-responsive nature of the p(PEGMA) network, to precisely regulate molecular transport. Under pH variations, the protonation and deprotonation of Ca-Alg network is controlled that regulate

anionic AD and cationic MB molecular transport. Under temperature variations, the hydrophobic behavior of the p(PEGMA) network controls the pore size on the hydrogel and molecular transport of RITC-Dextran with 10 kDa and 70 kDa molecular weights. By finely adjusting the MBAm concentration, we optimized the shell composition of the capsules, enhancing transport efficiency, mechanical strength and stability of the capsules under fluctuations in pH, temperature and mechanical stress, while preserving significant water content of the capsules' core. These properties make our hydrogel capsules ideal for various applications, such as sensors that detect and respond to environmental changes in real time, signaling changes in pH, temperature or mechanical stress. Similarly, as microreactors, these capsules could precisely control chemical reactions triggered by specific external stimuli.

CRediT authorship contribution statement

Hui Yang: Writing – original draft, Software, Methodology, Formal analysis, Data curation. **Catherine P. Whitby:** Writing – review & editing, Conceptualization. **Jadranka Travas-Sejdic:** Writing – review & editing, Supervision, Project administration, Funding acquisition.

Declaration of competing interest

The authors declare that they have no known competing financial interests or personal relationships that could have appeared to influence the work reported in this paper.

Data availability

Data will be made available on request.

Acknowledgements

This work was supported by the Reconfigurable Systems Research Programme of the MacDiarmid Institute for Advanced Materials and Nanotechnology.

Appendix A. Supplementary data

Supplementary data to this article can be found online at https://doi.org/10.1016/j.jcis.2024.08.119.

References

[1] E.M. Ahmed, Hydrogel: Preparation, characterization, and applications: a review, J. Adv. Res. 6 (2015) 105–121.
[2] M.E. Allen, J.W. Hindley, D.K. Baxani, O. Ces, Y. Elani, Hydrogels as functional components in artificial cell systems, Nat. Rev. Chem. 6 (2022) 562–578.
[3] M.C. Koetting, J.T. Peters, S.D. Steichen, N.A. Peppas, Stimulus-responsive hydrogels: theory, modern advances, and applications, Mater. Sci. Eng. R Rep. 93 (2015) 1–49.
[4] Z. Liu, W. Wang, R. Xie, X.J. Ju, L.Y. Chu, Stimuli-responsive smart gating membranes, Chem. Soc. Rev. 45 (2016) 460–475.
[5] H. Feng, N. Tang, M. An, R. Guo, D. Ma, X. Yu, J. Zang, N. Yang, Thermally-responsive hydrogels poly(N-isopropylacrylamide) as the thermal switch, J. Phys. Chem. C 123 (2019) 31003–31010.
[6] G. Kocak, C. Tuncer, V. Bütün, PH-Responsive polymers, Polym. Chem. 8 (2017) 144–176.
[7] L. Li, J.M. Scheiger, P.A. Levkin, Design and applications of photoresponsive hydrogels, Adv. Mater. 31 (2019).
[8] S. Murdan, Electro-responsive drug delivery from hydrogels, J. Control. Release 92 (2003) 1–17.
[9] M. Liang, D. Wei, Z. Yao, P. Ren, J. Dai, L. Xu, T. Zhang, Q. Zhang, Hydrogel adhesive formed via multiple chemical interactions: from persistent wet adhesion to rapid hemostasis, Biomater. Sci. 10 (2022) 1486–1497.
[10] J. Li, Z. Suo, J.J. Vlassak, Stiff, strong, and tough hydrogels with good chemical stability, J. Mater. Chem. B 2 (2014) 6708–6713.
[11] R.T. Shafranek, S.C. Millik, P.T. Smith, C.U. Lee, A.J. Boydston, A. Nelson, Stimuli-responsive materials in additive manufacturing, Prog. Polym. Sci. 93 (2019) 36–67.
[12] I. Tokarev, S. Minko, Stimuli-responsive porous hydrogels at interfaces for molecular filtration, separation, controlled release, and gating in capsules and membranes, Adv. Mater. 22 (2010) 3446–3462.
[13] N. Kumar, S. Singh, P. Sharma, B. Kumar, Single- dual-, and multi-stimuli-responsive nanogels for biomedical applications, Gels 10 (2024) 61.
[14] M.A. Haq, Y. Su, D. Wang, Mechanical properties of PNIPAM based hydrogels: a review, Mater. Sci. Eng. C 70 (2017) 842–855.
[15] S. Lee, W.M. Hamonangan, J.H. Kim, S.H. Kim, Soft and tough microcapsules with double-network hydrogel shells, Adv. Funct. Mater. 32 (2022) 1–11.
[16] S. Lee, B. Che, M. Tai, W. Li, S.H. Kim, Designing semipermeable hydrogel shells with controlled thickness through internal osmosis in triple-emulsion droplets, Adv. Funct. Mater. 31 (2021) 1–10.
[17] Y. Lu, Y. Chen, Y. Zhu, J. Zhao, K. Ren, Z. Lu, J. Li, Z. Hao, Stimuli-responsive protein hydrogels: their design, properties, and biomedical applications, Polymers (Basel). 15 (2023).
[18] S. Amirthalingam, A.K. Rajendran, Y.G. Moon, N.S. Hwang, Stimuli-responsive dynamic hydrogels: design, properties and tissue engineering applications, Mater. Horizons 10 (2023) 3325–3350.
[19] P.C. McCarthy, Y. Zhang, F. Abebe, Review recent applications of dual-stimuli responsive chitosan hydrogel nanocomposites as drug delivery tools, Molecules 26 (2021).
[20] Z. Bao, C. Xian, Q. Yuan, G. Liu, J. Wu, Natural polymer-based hydrogels with enhanced mechanical performances: preparation, structure, and property, Adv. Healthc. Mater. 8 (2019) 1–11.
[21] V.T. Tran, M.T.I. Mredha, I. Jeon, High-water-content hydrogels exhibiting superior stiffness, strength, and toughness, Extrem. Mech. Lett. 37 (2020) 100691.
[22] D.K. Nguyen, Y.M. Son, N. Lee, Hydrogel encapsulation of cells in core – shell microcapsules for cell delivery, Adv. Healthc. Mater. 4 (2015) 1537–1544.
[23] Y. Weng, Z. Song, C.H. Chen, H. Tan, Hybrid hydrogel reactor with metal–organic framework for biomimetic cascade catalysis, Chem. Eng. J. 425 (2021).
[24] I. Tokarev, S. Minko, Stimuli-responsive hydrogel thin films, Soft Matter 5 (2009) 511–524.
[25] T. Moragues, D. Arguijo, T. Beneyton, C. Modavi, K. Simutis, A.R. Abate, J.C. Baret, A.J. deMello, D. Densmore, A.D. Griffiths, Droplet-based microfluidics, Nat. Rev. Methods Prim. 3 (2023) 1–22.
[26] Q. Wu, X. Huang, R. Liu, X. Yang, G. Xiao, N. Jiang, D.A. Weitz, Y. Song, Multichannel multijunction droplet microfluidic device to synthesize hydrogel microcapsules with different core-shell structures and adjustable core positions, Langmuir 40 (2024) 1950–1960.
[27] S. Hardt, T. Hahn, Microfluidics with aqueous two-phase systems, Lab Chip 12 (2012) 434–442.
[28] T. Ahmed, C. Yamanishi, T. Kojima, S. Takayama, Aqueous two-phase systems and microfluidics for microscale assays and analytical measurements, Annu. Rev. Anal. Chem. 14 (2021) 231–255.
[29] B.U. Moon, D.K. Hwang, S.S.H. Tsai, Shrinking, growing, and bursting: microfluidic equilibrium control of water-in-water droplets, Lab Chip 16 (2016) 2601–2608.
[30] S. Daradmare, C.S. Lee, Recent progress in the synthesis of all-aqueous two-phase droplets using microfluidic approaches, Colloids Surf. B Biointerf. 219 (2022) 112795.
[31] W.F. Lai, A.S. Susha, A.L. Rogach, G. Wang, M. Huang, W. Hu, W.T. Wong, Electrospray-mediated preparation of compositionally homogeneous core-shell hydrogel microspheres for sustained drug release, RSC Adv. 7 (2017) 44482–44491.
[32] G. Chen, Y. Yu, X. Wu, G. Wang, G. Gu, F. Wang, J. Ren, H. Zhang, Y. Zhao, Microfluidic electrospray niacin metal-organic frameworks encapsulated microcapsules for wound healing, Research (2019).
[33] S. Zhao, P. Agarwal, W. Rao, H. Huang, R. Zhang, Z. Liu, J. Yu, N. Weisleder, W. Zhang, X. He, Coaxial electrospray of liquid core–hydrogel shell microcapsules for encapsulation and miniaturized 3D culture of pluripotent stem cells, Integr. Biol. 6 (2014) 874–884.
[34] D. Buenger, F. Topuz, J. Groll, Hydrogels in sensing applications, Prog. Polym. Sci. 37 (2012) 1678–1719.
[35] H. Tan, S. Guo, N.D. Dinh, R. Luo, L. Jin, C.H. Chen, Heterogeneous multi-compartmental hydrogel particles as synthetic cells for incompatible tandem reactions, Nat. Commun. 8 (2017) 1–10.
[36] H. Wang, Z. Zhao, Y. Liu, C. Shao, F. Bian, Y. Zhao, Biomimetic enzyme cascade reaction system in microfluidic electrospray microcapsules, Sci. Adv. 4 (2018) eaat2816.
[37] Y. Elani, R.V. Law, O. Ces, Vesicle-based artificial cells as chemical microreactors with spatially segregated reaction pathways, Nat. Commun. 5 (2014) 1–5.
[38] D.; Poncelet, R.J.; Neufeld, M.F.A. Goosen, B.; Burgarski, V.; Babak, Formation of microgel beads by electric dispersion of polymer solutions, 1999.
[39] A. Jaworek, A.T. Sobczyk, A. Krupa, Electrospray application to powder production and surfae coating, J. Aerosol Sci. 125 (2018) 57–92.
[40] K.Y. Lee, D.J. Mooney, Alginate: properties and biomedical applications, Prog. Polym. Sci. 37 (2012) 106–126.
[41] E. Martwong, Y. Tran, Lower critical solution temperature phase transition of poly (PEGMA) hydrogel thin films, Langmuir 37 (2021) 8585–8593.
[42] H. Choukaife, A.A. Doolaanea, M. Alfatama, Alginate nanoformulation: Influence of process and selected variables, 2020.
[43] J. Travas-Sejdic, A. Easteal, Swelling equilibria and volume phase transition of polyelectrolyte gel with strongly dissociated groups, Polym. Gels Networks 5 (1998) 481–502.
[44] N.S. Tomović, K.T. Trifković, M.P. Rakin, M.B. Rakin, B.M. Bugarski, ‘, Chem. Ind. Chem. Eng. Q. 21 (2015) 411–417.
[45] W.P. Voo, C.W. Ooi, A. Islam, B.T. Tey, E.S. Chan, Calcium alginate hydrogel beads with high stiffness and extended dissolution behaviour, Eur. Polym. J. 75 (2016) 343–353.

[46] J. Claus, A. Brietzke, C. Lehnert, S. Oschatz, N. Grabow, U. Kragl, Swelling characteristics and biocompatibility of ionic liquid based hydrogels for biomedical applications, PLoS One 15 (2020).
[47] J. Li, D.J. Mooney, Designing hydrogels for controlled drug delivery, Nat. Rev. Mater. 1 (2016) 1–17.
[48] A.K. Bhattacharya, C. Venkobachar, Removal of Cadmium (II) by Low Cost Adsorbents, J. Environ. Eng. 110 (1984) 110–122.
[49] Y.S. Ho, G. McKay, Pseudo-second order model for sorption processes, Process Biochem. 34 (1999) 451–465.
[50] F.C. Wu, R.L. Tseng, R.S. Juang, Initial behavior of intraparticle diffusion model used in the description of adsorption kinetics, Chem. Eng. J. 153 (2009) 1–8.
[51] F.C. Wu, R.L. Tseng, R.S. Juang, Characteristics of Elovich equation used for the analysis of adsorption kinetics in dye-chitosan systems, Chem. Eng. J. 150 (2009) 366–373.
[52] V. Vadivelan, K. Vasanth Kumar, Equilibrium, kinetics, mechanism, and process design for the sorption of methylene blue onto rice husk, J. Colloid Interface Sci. 286 (2005) 90–100.
[53] A.T. Paulino, M.R. Guilherme, A.V. Reis, G.M. Campese, E.C. Muniz, J. Nozaki, Removal of methylene blue dye from an aqueous media using superabsorbent hydrogel supported on modified polysaccharide, J. Colloid Interface Sci. 301 (2006) 55–62.
[54] A.F. Hassan, A.M. Abdel-Mohsen, M.M.G. Fouda, Comparative study of calcium alginate, activated carbon, and their composite beads on methylene blue adsorption, Carbohydr. Polym. 102 (2014) 192–198.
[55] B. Bestani, N. Benderdouche, B. Benstaali, M. Belhakem, A. Addou, Methylene blue and iodine adsorption onto an activated desert plant, Bioresour. Technol. 99 (2008) 8441–8444.
[56] J.P. Byers, J.G. Sarver, Pharmacokinetic Modeling, first ed.,, Elsevier Inc., 2009.
[57] C. Aharoni, F.C. Tompkins, Kinetics of adsorption and desorption and the elovich equation, Adv. Catal. 21 (1970) 1–49.
[58] S. Lee, X. Tong, F. Yang, The effects of varying poly(ethylene glycol) hydrogel crosslinking density and the crosslinking mechanism on protein accumulation in three-dimensional hydrogels, Acta Biomater. 10 (2014) 4167–4174.
[59] J. Travas-Sejdic, A.J. Easteal, Effect of crosslink density and amount of charges on poly(acrylamide-co- 2-acrylamido-2-methyl-1-propanesulphonic acid) gel structure, Polymer (guildf). 41 (2000) 2535–2542.
[60] J. Travas-Sejdic, A. Easteal, R. Knott, J.S. Pedersen, Small-angle neutron scattering from poly(NIPA-co-AMPS) gels, J. Appl. Crystallogr. 33 (2000) 735–739.
[61] D. Zhang, F. Yang, J. He, L. Xu, T. Wang, Z.Q. Feng, Y. Chang, X. Gong, G. Zhang, J. Zheng, Multiple physical bonds to realize highly tough and self-adhesive double-network hydrogels, ACS Appl. Polym. Mater. 2 (2020) 1031–1042.
[62] J. Ma, J. Luo, Y. Liu, Y. Wei, T. Cai, X. Yu, H. Liu, C. Liu, J.C. Crittenden, Pb(ii), Cu (ii) and Cd(ii) removal using a humic substance-based double network hydrogel in individual and multicomponent systems, J. Mater. Chem. A 6 (2018) 20110–20120.
[63] S. Zu, Z. Zhang, Q. Liu, Z. Wang, Z. Song, Y. Guo, Y. Xin, S. Zhang, 4D printing of core–shell hydrogel capsules for smart controlled drug release, Bio-Design Manuf. 5 (2022) 294–304.
[64] M.R. de Moura, F.A. Aouada, M.R. Guilherme, E. Radovanovic, A.F. Rubira, E. C. Muniz, Thermo-sensitive IPN hydrogels composed of PNIPAAm gels supported on alginate-Ca2+ with LCST tailored close to human body temperature, Polym. Test. 25 (2006) 961–969.
[65] H. Zhang, Y. Zhang, L. He, B. Yang, S. Zhu, M. Yao, Thermal-responsive poly(N-isopropyl acrylamide)/sodium alginate hydrogels: preparation, swelling behaviors, and mechanical properties, Colloid Polym. Sci. 294 (2016) 1959–1967.
[66] J.F. Lutz, Polymerization of oligo(ethylene glycol) (meth)acrylates: toward new generations of smart biocompatible materials, J. Polym. Sci. Part A Polym. Chem. 46 (2008) 3459–3470.
[67] F. Wang, Z. Sun, X. Li, K. Wang, D. Chen, Z. Li, Study on factors influencing the viscosity of sodium carboxymethyl cellulose used in capsule-mucous sealers, Geofluids 1 (2022).